

WEBPII: BENCHMARKING VISUAL PII DETECTION FOR COMPUTER-USE AGENTS

Nathan Zhao

Stanford University

nathanzh@stanford.edu

ABSTRACT

Computer use agents create new privacy risks: training data collected from real websites inevitably contains sensitive information, and cloud-hosted inference exposes user screenshots. Detecting personally identifiable information in web screenshots is critical for privacy-preserving deployment, but no public benchmark exists for this task. We introduce WEBPII, a fine-grained synthetic benchmark of 44,865 annotated e-commerce UI images designed with three key properties: extended PII taxonomy including transaction-level identifiers that enable reidentification, anticipatory detection for partially-filled forms where users are actively entering data, and scalable generation through VLM-based UI reproduction. Experiments validate that these design choices improve layout-invariant detection across diverse interfaces and generalization to held-out page types. We train WEBREDACT to demonstrate practical utility, more than doubling text-extraction baseline accuracy (0.753 vs 0.357 mAP@50) at real-time CPU latency (20ms). We release the dataset and trained model to support privacy-preserving computer use research.

1 INTRODUCTION

Computer use agents—language models that operate graphical user interfaces through vision and action—represent a significant capability advance toward general-purpose AI assistants. Unlike traditional web automation that operates on structured HTML or APIs, vision-based systems observe rendered web pages as images and produce mouse and keyboard actions to accomplish user goals. Recent systems such as Claude Computer Use Anthropic (2024) and Gemini 2.5 Comanici et al. (2025) demonstrate purely vision-driven agents that can book flights, complete checkout flows, navigate e-commerce sites, and manage user accounts across arbitrary websites without access to DOM structure. As these systems scale from research prototypes to production deployments serving millions of sessions, their visual-first architecture creates fundamental privacy problems: every screenshot observation contains rendered PII, and standard cloud-hosted inference exposes sensitive user data during routine operation.

The privacy challenges span both training and inference. Training data collected from real websites inevitably contains PII that models memorize and leak Lukas et al. (2023); Nasr et al. (2023), while cloud-hosted inference routinely exposes user screenshots. Existing mitigations are insufficient: sandboxed benchmarks Zhou et al. (2023); Xie et al. (2024) use fabricated data that does not transfer to real sessions, crowdsourced datasets Deng et al. (2023); Lù et al. (2024) lack real-time authenticated content, agentic pipelines Wang et al. (2025d) lack visual PII detection, and federated approaches Wang et al. (2025c;b) still leak information through gradient updates.

Critically, **no public benchmark exists for visual PII detection in web interfaces**. Text-based PII systems Microsoft (2024b); ai4Privacy (2023); Selvam & Ghosh (2025) operate on extracted strings, missing rendered content where sensitivity derives from visual context rather than surrounding words. Document-focused datasets Bulatov et al. (2021); Lerouge et al. (2024) target fixed-layout identity documents with predictable field positions. Scene text datasets Veit et al. (2016); Gupta et al. (2016) localize text without distinguishing sensitive content from UI chrome.

This paper presents a dataset-first contribution to address this gap. We introduce WEBPII, a fine-grained synthetic benchmark of e-commerce interface images designed with properties essential for visual PII detection in web interfaces. Our experiments validate key design choices—fill state

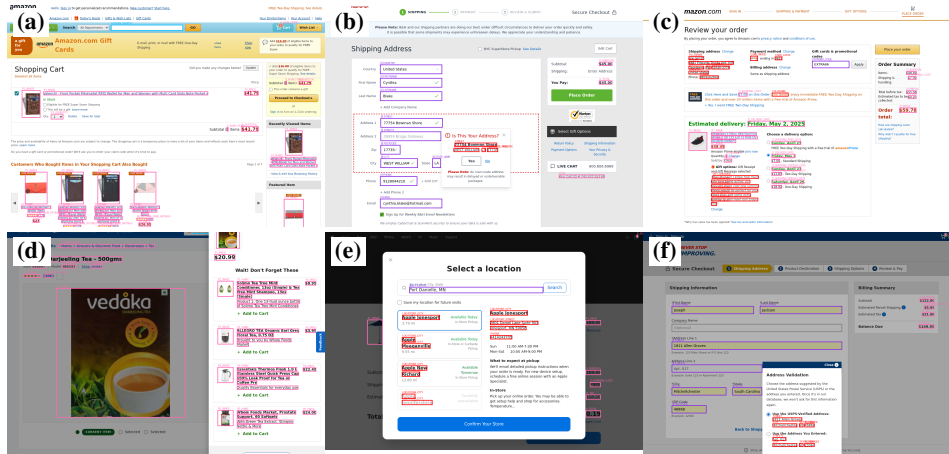


Figure 1: Sample images from WEBPII, rendered with different injected data. The dataset captures the visual complexity of e-commerce interfaces: variable page heights reflecting diverse checkout flows and product displays (compare compact cart in (a) with extended layout in (d)), input fields and dropdown selectors, modal overlays with backdrops that occlude underlying content, ad hoc identifying information such as gift messages (c) and proposed pickup locations (e), and derived values requiring computation of taxes and totals. Bounding boxes respect occlusion boundaries. Pink indicates product annotations, purple denotes empty input fields, and red identifies PII.

diversity, data injection density, extended identifier taxonomy—demonstrating that the dataset enables layout-invariant PII detection across diverse e-commerce layouts.

Figure 1 illustrates the diversity of PII contexts across e-commerce layouts that we can dynamically vary through data injection. Beyond this visual diversity, the dataset introduces three validated properties:

1. **Extended PII taxonomy.** Beyond traditional PII, WEBPII annotates *extended identifiers*—order numbers, tracking IDs, delivery dates, purchase histories—that enable re-identification but fall outside conventional PII definitions.
2. **Anticipatory detection.** Web interfaces expose PII as it is being typed. WEBPII generates annotations at each progressive state of form-filling, enabling models to trigger redaction proactively rather than after sensitive data is fully visible.
3. **Scalable generation pipeline.** Our VLM-based approach dynamically generates diverse layouts and injects varied PII configurations, producing pixel-level bounding boxes without manual annotation.

Our generation pipeline exploits VLM-based UI reproduction Anthropic (2025a); SST (2025) to generate functional frontend code from screenshots, embedding annotation attributes during code generation for programmatic bounding box extraction. Section 2.1 documents the PII taxonomy underlying our annotations.

We validate the dataset’s utility by training **WEBREDACT**, a visual detection model that more than doubles text-extraction baseline accuracy (0.753 vs. 0.357 mAP@50) at real-time CPU latency (20ms). Section 3 presents ablation studies validating our design choices.

We release WEBPII, WEBREDACT, and WEBREDACT-LARGE to support development of privacy-preserving computer use systems.¹

¹Dataset and model available at: <https://webpii.github.io/>

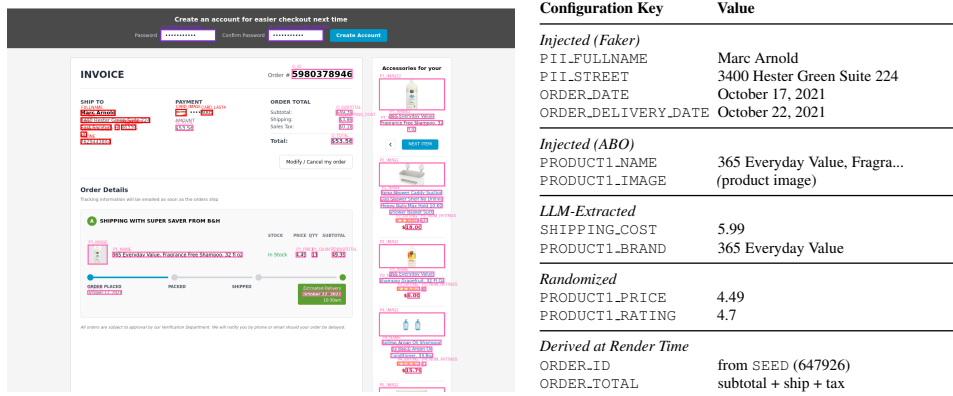


Figure 2: Data injection maps configuration values to rendered UI elements. Left: annotated screenshot with bounding boxes. Right: selected subset of data injected for this page—Faker-generated PII, ABO product data, LLM-extracted metadata, and values derived at render time. The same layout rendered with different configurations produces diverse training examples with automatic annotations.

2 THE WEBPII DATASET

E-commerce interfaces present PII challenges distinct from documents or scene text. While an email address in a scanned form appears as static pixels, the same email in a web UI may be rendered through JavaScript, styled with CSS, and wrapped in interactive elements. Moreover, web forms require *anticipatory detection*—identifying sensitive fields before users finish typing, as privacy interventions should trigger during entry rather than after completion. Beyond traditional PII, these interfaces expose *extended identifiers*—order IDs, tracking numbers, delivery dates—that enable reidentification despite not constituting traditional PII. Our benchmark must capture this complexity.

Generating annotated PII data at scale presents a dilemma: real screenshots contain real PII requiring manual annotation, while synthetic generation risks unrealistic layouts. We resolve this through *reproduction with annotation injection*: collecting real e-commerce screenshots, then using vision-language models to recreate them as functional code with annotations embedded during generation. This produces pixel-accurate bounding boxes without manual labeling.

2.1 EXTENDED IDENTIFIERS IN E-COMMERCE

Beyond traditional PII (names, addresses, payment details), e-commerce interfaces display transaction-level attributes—order dates, merchants, item quantities, financial totals, delivery information—that enable reidentification despite not constituting traditional PII. Four credit card transactions containing just the merchant and date reidentify 90% of 1.1M users de Montjoye et al. (2015); eight movie ratings with dates reidentify 99% of Netflix users Narayanan & Shmatikov (2008). Cross-platform attacks link accounts by matching transaction patterns Archie et al. (2018).

These identifiers also reveal sensitive personal attributes—purchase patterns predict health conditions Aiello et al. (2019); Sasaya et al. (2026), socioeconomic status Hashemian et al. (2017), and personal characteristics Duhigg & Pole (2012); Kosinski et al. (2013)—informing insurance underwriting Allen (2018), data broker segmentation Callanan et al. (2021), and surveillance Tokson (2024); Kerr (2021); Sobel (2023).

E-commerce interfaces also expose fields that are directly identifying yet absent from existing PII benchmarks: gift messages contain both sender and recipient names alongside personal notes; B2B purchase order numbers link individuals to corporate procurement systems and company names; delivery security codes enable package retrieval. Visual PII detection for agentic commerce must address these fields alongside traditional PII.

2.2 DATA COLLECTION AND GENERATION

We collected screenshots from 10 e-commerce brands across 19 page types—account dashboards, order history, order tracking, checkout flows, cart, billing address, delivery options, payment entry, gifting, store pickup, and product pages. Selection prioritized layouts exhibiting complex UI patterns: modal overlays, dynamic sidebars, embedded maps for store locators, cluttered multi-step forms, and responsive designs. We source multiple distinct layouts, including both current designs and prior designs that remain accessible, and so on, yielding 408 unique layouts. All of these original screenshots serve as visual targets for reproduction; we do not use them directly in the dataset.

For generation, we evaluated GPT-5.2 OpenAI (2025) with OpenCode SST (2025) and Claude Opus 4.5 Anthropic (2025b) with Claude Code Anthropic (2025a); Claude exhibited superior rule-following on annotation conventions, requiring fewer iterations to reliably apply the schema.

The model generates React components, reproducing each screenshot with two enforced constraints: (1) all PII and product information must reference data variables rather than hardcoded values, and (2) every sensitive element must include a data attribute for annotation extraction. A Vite You (2024) development server renders each component, and a Playwright Microsoft (2024a) harness captures screenshots while extracting bounding boxes for all attributed elements via DOM queries. We provide the model with common e-commerce assets—company and payment method logos, security badges, shipping carrier icons, user avatar images, and map tiles—and pre-install icon libraries (Lucide, Heroicons, Phosphor) to avoid token-heavy inline SVG generation.²

Generating accurate reproductions requires decomposing the task into specialized prompts, with context cleared between stages to prevent degradation. The pipeline proceeds in four stages: (1) *structure*, where the model generates a React component from the source screenshot, replacing all PII and product information with data variable references; (2) *attribute marking*, where a second pass tags each reference with annotation attributes for bounding box extraction; (3) *input handling*, where form fields are configured for partial-fill simulation (Section 2.4); and (4) *visual refinement*, where the rendered output is compared against the source in partitioned regions, with targeted fixes applied only to sections with discrepancies.

Beyond reproduction, the model extracts shipping costs and tax rates from source screenshots, derives order totals from item quantities, and infers platform-specific identifier formats. Human-in-the-loop validation corrects 39% of layouts (viewport overflow, missing markup, initialization errors) via natural language instructions that delegate fixes back to Claude, typically requiring 1–2 iterations for any fixes. This validation amortizes across 25 data variants and all progressive fill states per layout. Section B provides more details on cost, human time spent handling, and decisions involved in creating the annotation pipeline.

2.2.1 DATA INJECTION

The generated React components contain variable references rather than hardcoded values. At render time, data configurations populate these references with values from multiple sources: synthetic PII, product data, and attributes extracted or computed during generation. This enables the same layout to produce diverse screenshots with automatic annotations. We define three annotation types—`pii`, `product`, and `order`—corresponding to data attributes in our generation schema, illustrated in Figure 2:

PII annotations (`data-pii`) cover traditional PII and context-specific fields. Values are generated via Faker Faraglia (2024) with locale-appropriate formatting; context-specific fields (delivery instructions, security codes) use templated generation matching observed platform conventions.

Product annotations (`data-product`) capture displayed merchandise: names, descriptions, prices, images, ratings, and quantities. Product images are sourced from Amazon Berkeley Objects Collins et al. (2021) (~147K products, 400K images). Since ABO products oftentimes lack well-structured metadata, we clean the dataset for site-specific identifiers, placeholder images, and use GPT-4o-mini OpenAI (2024) to extract brand names and item categories from titles and descriptions. For “recommended” and “frequently bought together” sections, we use fuzzy matching over

²User avatars sourced from xsgames.co/randomusers/; map tiles from openstreetmap.org (© OpenStreetMap contributors, ODbL).

Figure 3 shows two screenshots of a form, labeled (a) and (b).
 (a) Partial: This form is partially filled. The 'Country/Region' dropdown is set to 'United States'. The 'Full name (First and Last name)' field contains 'April Garrison'. The 'Phone number' field contains '2055486874'. The 'Address' field contains '84210 Alexis Turnpike' and '277 Lisa Circles Suite 043'. The 'City' field contains 'New M', which is highlighted in yellow. The 'State' dropdown is set to 'Select' and the 'ZIP Code' field is empty. A checkbox at the bottom is labeled 'Make this my default address'.
 (b) Empty: This form is empty. The 'Country/Region' dropdown is set to 'Select a Country'. The 'Full name (First and Last name)' field contains the placeholder text 'Full name (First and Last name)'. The 'Phone number' field contains the placeholder text 'Phone number'. The 'Address' field contains the placeholder text 'Street address or P.O. Box' and 'Apt, suite, unit, building, floor, etc.'. The 'City' field contains the placeholder text 'City'. The 'State' dropdown is set to 'Select' and the 'ZIP Code' field is empty. A checkbox at the bottom is labeled 'Make this my default address'.

Figure 3: Form fill states for anticipatory detection. (a) Partial: mid-entry state with later fields incomplete (city field shows “New M” mid-typing). (b) Empty: pristine form with placeholder text and input field annotations. Yellow indicates partially filled fields; grey denotes empty fields.

product descriptions to retrieve semantically similar items. Values not provided by Faker or ABO are programmatically generated to follow realistic patterns, including review counts, ratings, and delivery dates.

Order annotations (`data-order`) capture extended identifiers: order IDs, dates, tracking numbers, and financial totals. Order IDs and tracking numbers use seeded pseudo-random generation with platform-specific format templates. Shipping costs and tax percentages are extracted from the source screenshot during UI reconstruction, preserving realistic values for each layout. As shown in Figure 2, derived values such as order subtotals and totals are computed at render time; the generation model must recognize these as derived and apply appropriate attributes.

Additional fields are generated via GPT-4o-mini when building data configuration files to produce realistic content: navigation breadcrumbs referencing browsing history (Figure 1d), gift messages mentioning both recipient names and purchased items (Figure 1c), and promotional copy. Each component C_i is rendered with $m = 25$ distinct data configurations, producing diverse screenshots with varied PII values, product images, and transaction details while maintaining automatic annotation alignment through DOM queries.

2.3 ANNOTATION EXTRACTION

By requiring data attributes during generation, we extract pixel-coordinate bounding boxes directly from the rendered DOM using the browser’s Range API to match text content with PII values. Wrapped text is split into separate bounding boxes per line via vertical overlap detection. This approach adapts to responsive layouts and ensures derived values receive proper attribution. Our extraction pipeline performs visibility analysis, excluding fully occluded elements and clipping partially visible ones to their visible extent.

2.4 ANTICIPATORY DETECTION

A key differentiator from text-based PII datasets is our support for *anticipatory detection*—identifying PII before the user has finished typing. In deployed systems, privacy-preserving interventions should trigger as sensitive data is being entered, not after completion. For each component C_i containing N_i form fields, we generate anticipatory variants across progressive fill states: for stage k (where $1 \leq k < N_i$), fields 1 through $k - 1$ are fully filled, field k is partially filled (mid-typing), and fields $k + 1$ through N_i remain empty. Figure 3 illustrates two stages of this progression.

This systematic progression mirrors actual user interaction and ensures balanced representation across fill states. Models observe each field in three contexts: empty (before the user reaches it), partially filled (active input), and fully filled (after completion). Rather than biasing towards any particular fill state, the dataset provides equal exposure to all stages of form completion. Additionally, forms with optional fields are rendered with these fields randomly included or excluded across data injections, exposing models to structural variability in form layouts.

2.5 SUMMARY AND COMPARISON

WEBPII comprises 44,865 images spanning 10 e-commerce websites and 19 distinct page types, with 993,461 total bounding box annotations. This includes 10,200 base images with fully-filled forms, augmented by our anticipatory detection methodology that generates 28,653 partial-fill variants and 6,012 empty-form variants. Annotations span three categories (PII, product information, and order identifiers) across diverse HTML contexts (rendered text, input fields, and images). Detailed breakdowns of annotation density, category distribution, HTML element types, company distribution, and page type distribution appear in Appendix A.

WEBPII is the first benchmark combining visual localization with semantic PII categories on rendered web interfaces, while annotating extended identifiers absent from prior work. Table 2 summarizes these distinctions.

3 EXPERIMENTS

3.1 EXPERIMENTAL SETUP

3.1.1 DATA SPLITS

The diversity of WEBPII enables evaluation of generalization at different levels. We render each of the 408 unique layouts with 25 data injection variants (different PII values, addresses, and product information), and for layouts with input fields, generate the fill states described in Section 2.4: *full*, *partial*, and *empty*. We evaluate three split strategies: **Test**_{Cross-Page} holds out 20% of layouts randomly (82 layouts, 298 fill states), testing whether models learn layout-invariant features within a company’s design system. **Test**_{Cross-Company} holds out all Amazon layouts (56 layouts, 152 fill states) while training on 11 other companies (352 layouts, 1,416 fill states), evaluating generalization to entirely new visual styles and brand identities. **Test**_{Cross-Type} holds out all receipt pages (20 layouts, 50 fill states) while training on 18 other page types (388 layouts, 1,518 fill states), measuring whether detection strategies transfer across functionally different page categories with distinct UI patterns. For all splits, we ensure no data leakage: the specific PII values, addresses, and product information in test images never appear in training.

3.2 BASELINE METHODS

3.2.1 TEXT-BASED METHODS

We evaluate text-based baselines using a two-stage pipeline: (1) OCR extraction to obtain text spans with bounding boxes, (2) classification to identify sensitive content. This approach mirrors existing PII detection systems that operate on extracted text rather than raw pixels. We compare three approaches: Presidio Microsoft (2024b), an NER-based system using pattern matching and named entity recognition; GPT-4o-mini for LLM-based classification; and document understanding models LayoutLMv3 Huang et al. (2022) and Donut Kim et al. (2021) that encode visual layout alongside text. All document understanding pipelines use GPT-4o-mini for final classification to ensure fair comparison. We evaluate multiple OCR engines Tesseract Smith (2007), EasyOCR JaidedAI (2024), and PaddleOCR Cui et al. (2025), reporting the highest-accuracy configuration (LayoutLMv3) and fastest configuration (Tesseract + Presidio). Note that text-based approaches can only evaluate text content—product images are excluded as OCR provides no signal for visual elements. Appendix D.1 presents detailed ablations across all OCR engines, language models, and classification approaches.

3.2.2 WEBREDACT

We train object detection models on WEBPII as WEBREDACT, targeting real-time inference suitable for live redaction. While WEBPII contains fine-grained annotations for different PII types, we train on two classes grouped by visual appearance: `text` (all text-based elements including PII fields, product descriptions, and order information) and `image` (product images). This simplification improves detection reliability by providing more training examples per class and clearer visual distinctions between categories. Training uses 100 epochs, batch size 16, with standard augmentations (random crops, flips, color jittering). We train two model variants: WEBREDACT at 640×640 resolution for

Table 1: Baseline results on $\text{Test}_{\text{Cross-Company}}$ (Amazon, full-fill images only). OCR+Presidio uses Tesseract; LayoutLMv3 uses GPT-4o-mini for classification.

METHOD	MAP@50	LATENCY
OCR + PRESIDIO	0.183	1.3s
LAYOUTLMV3 + GPT-4O-MINI	0.357	2.9s
WEBREDACT (OURS)	0.753	20MS
WEBREDACT-LARGE (OURS)	0.842	312MS

real-time CPU inference, and WEBREDACT-LARGE at 1280×1280 resolution for higher accuracy when near-real-time constraints can be relaxed.

3.3 RESULTS

Table 1 presents main results on $\text{Test}_{\text{Cross-Company}}$, evaluating generalization to entirely new visual styles without seeing Amazon’s design system during training. We evaluate text-based baselines only on full-filled images, as these approaches cannot identify empty or partially-filled input fields. Even on this favorable subset, both WEBREDACT variants substantially outperform text-based methods: WEBREDACT achieves 0.753 mAP@50, more than double the best text-based baseline (LayoutLMv3 at 0.357), while WEBREDACT-LARGE reaches 0.842 mAP@50. Detailed failure mode analysis for OCR+LLM systems appears in Appendix D.1.

WEBREDACT processes images in $\sim 20\text{ms}$ on mid-range consumer CPUs (Intel i5/AMD Ryzen 5), meeting real-time constraints for 30fps redaction, while WEBREDACT-LARGE requires $\sim 312\text{ms}$ ($\sim 3\text{fps}$). Both models use OpenVINO for CPU inference. Text-based methods are substantially slower: Tesseract Smith (2007) OCR extraction alone (453ms, excluding classification) is slower than WEBREDACT-LARGE’s full detection pipeline.

3.4 DATASET ABLATIONS

We conduct ablations to validate WEBPII’s design choices; full tables appear in Appendix D.

Split strategies. We compare three split strategies (Table 13). $\text{Test}_{\text{Cross-Page}}$ achieves 0.797 mAP@50, indicating models learn layout-invariant features within a company’s design system. $\text{Test}_{\text{Cross-Company}}$ degrades to 0.753 when generalizing to Amazon’s distinct visual style. $\text{Test}_{\text{Cross-Type}}$ shows the largest degradation (0.728), revealing that page-type-specific patterns transfer less effectively than company-specific design conventions.

Fill state diversity. Training on full screenshots alone achieves 0.771 mAP@50 (Table 14). Adding empty screenshots *without* partials degrades performance to 0.758, while full+partial achieves 0.797 (+0.026). Combining all three states achieves 0.825 mAP@50, demonstrating that partial fills provide essential intermediate visual grounding.

Progressive fill density. Increasing partial-fill stages per layout from 1 to 5 improves performance from 0.758 to 0.802 mAP@50 (Table 15), with the strongest gains on partial-fill test images (0.774 to 0.835). Each additional stage exposes the model to new intermediate form states, providing non-redundant learning signal for field detection across the full spectrum of user interaction.

Text variant density. Increasing text variants per layout from 1 to 25 improves performance from 0.795 to 0.820 mAP@50 (Table 16). Both precision and recall increase with more variants (0.805 to 0.842 and 0.713 to 0.731 respectively), confirming that diverse data injections—varying names, addresses, and products—improve generalization beyond layout diversity alone.

4 DISCUSSION

4.1 WHY CPU-FIRST DETECTION

Our emphasis on lightweight CPU-executable models reflects deployment constraints for privacy-sensitive applications: on-device processing keeps screen content local rather than transmitting to

cloud APIs Zhou et al. (2019), continuous detection must not overload local compute, and high-volume scenarios (browser extensions, OS-level privacy layers) make per-inference GPU costs prohibitive. This aligns with broader trends toward on-device computer use agents Awadallah et al. (2025); Wang et al. (2025a); Lin et al. (2024), where privacy-preserving detection must operate within the same resource envelope.

4.2 LIMITATIONS AND FUTURE WORK

Several limitations suggest directions for future work: domain scope is restricted to English-language e-commerce interfaces, with extension to other languages and domains (banking, healthcare, social media) requiring additional data collection; static image annotation does not capture challenges present in video streams with scrolling and state transitions; and our PII taxonomy conservatively labels all products and order identifiers as potentially identifying, which may cause over-redaction without contextual understanding.

Beyond privacy protection, WEBPII enables applications in computer use agent systems. PII, product, and input region detection provides semantic grounding for agent inference—extending GUI grounding approaches Lu et al. (2024); Cheng et al. (2024); Gou et al. (2024); Yang et al. (2023); Awadalla et al. (2025); Feizi et al. (2025) to allow agents to condition behavior on field sensitivity. The synthetic generation pipeline’s controllability could enable RL environment construction for agent training, where programmatic trajectory specification Pahuja et al. (2025); Wang et al. (2025e) enables scalable production of training data compared to expensive manual demonstration Deng et al. (2023); Lù et al. (2024).

5 CONCLUSION

We introduced WEBPII, a fine-grained synthetic benchmark for visual PII detection in web interfaces, designed with three validated properties: extended PII taxonomy including transaction-level identifiers, anticipatory detection for partially-filled forms, and scalable generation through VLM-based UI reproduction. Our generation pipeline produces annotated data at scale by instrumenting LLM-driven UI reproduction with programmatic annotation extraction, requiring human validation for 39% of layouts. Ablation studies validate these design choices, confirming that fill state diversity and data injection density each provide significant gains across split strategies.

We trained WEBREDACT to validate practical utility: the model more than doubles text-extraction baseline accuracy (0.753 vs 0.357 mAP@50) while achieving real-time CPU inference (20ms). As computer use agents transition from research prototypes to deployed systems, WEBPII provides a foundation for integrating privacy protection into their design. We release the dataset and model to support privacy-preserving computer use research.

IMPACT STATEMENT

This work aims to improve privacy in computer use systems by enabling automated detection and redaction of sensitive information in web interfaces. While PII detection models could theoretically be misused for surveillance, actors with such intent can already extract PII through existing methods (foundation models, offline OCR) that do not require real-time visual localization. The availability of privacy-protective tools for the broader research community represents a net positive for user privacy.

REFERENCES

- ai4Privacy. pii-masking-43k (Revision c47c98d), 2023. URL <https://huggingface.co/datasets/ai4privacy/pii-masking-43k>.
- L. Aiello, Rossano Schifanella, D. Quercia, and Lucia Del Prete. Large-scale and high-resolution analysis of food purchases and health outcomes. *EPJ Data Science*, 8, 2019.
- Marshall Allen. Health insurers are vacuuming up details about you — and it could raise your rates. ProPublica, July 2018. URL <https://www.propublica.org/article/health-insurers-are-vacuuming-up-details-about-you-and-it-could-raise-your-rates>.

- Anthropic. Claude 3 Model Card Addendum: October 2024, 10 2024. URL <https://assets.anthropic.com/m/1cd9d098ac3e6467/original/Claude-3-Model-Card-October-Addendum.pdf>. Introducing computer use capability in Claude 3.5 Sonnet.
- Anthropic. Claude Code, 2025a. URL <https://github.com/anthropics/claude-code>.
- Anthropic. System Card: Claude Opus 4.5. Technical report, Anthropic, November 2025b. URL <https://assets.anthropic.com/m/64823ba7485345a7/Claude-Opus-4-5-System-Card.pdf>.
- Maryam Archie, Sophie Gershon, Abigail Katcoff, and Aileen Zeng. Who ’ s watching ? de-anonymization of netflix reviews using amazon reviews. 2018.
- Anas Awadalla, Dhruva Ghosh, Aylin Akkus, Yuhui Zhang, Marianna Nezhurina, Jenia Jitsev, Yejin Choi, and Ludwig Schmidt. Gelato — From Data Curation to Reinforcement Learning: Building a Strong Grounding Model for Computer-Use Agents. <https://github.com/mlfoundations/gelato>, 2025.
- Ahmed Awadallah, Yash Lara, Raghav Magazine, Hussein Mozannar, Akshay Nambi, Yash Pandya, Aravind Rajeswaran, Corby Rosset, Alexey Taymanov, Vibhav Vineet, Spencer Whitehead, and Andrew Zhao. Fara-7B: An Efficient Agentic Model for Computer Use, 2025.
- K. Bulatov, E. Emelianova, D. Tropin, N. Skoryukina, Y. Chernyshova, A. Sheshkus, S. Usilin, Zuheng Ming, J. Burie, M. Luqman, and V. Arlazarov. MIDV-2020: A Comprehensive Benchmark Dataset for Identity Document Analysis. *ArXiv*, abs/2107.00396, 2021.
- G. Callanan, David F. Perri, and Sandra M. Tomkowicz. Targeting vulnerable populations: The ethical implications of data mining, automated prediction, and focused marketing. *Business and Society Review*, 2021.
- Kanzhi Cheng, Qiushi Sun, Yougang Chu, Fangzhi Xu, Yantao Li, Jianbing Zhang, and Zhiyong Wu. SeeClick: Harnessing GUI Grounding for Advanced Visual GUI Agents. pp. 9313–9332, 2024.
- Jasmine Collins, Shubham Goel, Achleshwar Luthra, Leon L. Xu, Kenan Deng, Xi Zhang, T. F. Y. Vicente, H. Arora, T. Dideriksen, M. Guillaumin, and J. Malik. ABO: Dataset and Benchmarks for Real-World 3D Object Understanding. In *2022 IEEE/CVF Conference on Computer Vision and Pattern Recognition (CVPR)*, pp. 21094–21104, 2021.
- Gheorghe Comanici, Eric Bieber, Mike Schaekermann, Ice Pasupat, Noveen Sachdeva, Inderjit Dhillon, Marcel Blistein, Ori Ram, Dan Zhang, Evan Rosen, Luke Marris, Sam Petulla, Colin Gaffney, A. Aharoni, Nathan Lintz, T. C. Pais, Henrik Jacobsson, Idan Szpektor, Nan-Jiang Jiang, Krishna Haridasan, Ahmed Omran, Nikunj Saunshi, Dara Bahri, Gaurav Mishra, Eric Chu, et al. Gemini 2.5: Pushing the frontier with advanced reasoning, multimodality, long context, and next generation agentic capabilities. *ArXiv*, abs/2507.06261, 2025.
- Cheng Cui, Ting Sun, Manhui Lin, Tingquan Gao, Yubo Zhang, Jiakuan Liu, Xueqing Wang, Zelun Zhang, Changda Zhou, Hongen Liu, Yue Zhang, Wenyu Lv, Kui Huang, Yichao Zhang, Jing Zhang, Jun Zhang, Yi Liu, Dianhai Yu, and Yanjun Ma. PaddleOCR 3.0 Technical Report, 2025. URL <https://arxiv.org/abs/2507.05595>.
- Yves-Alexandre de Montjoye, Laura Radaelli, Vivek Kumar Singh, and Alex Pentland. Unique in the Shopping Mall: On the Reidentifiability of Credit Card Metadata. *Science*, 347(6221):536–539, 2015.
- Xiang Deng, Yu Gu, Boyuan Zheng, Shijie Chen, Samuel Stevens, Boshi Wang, Huan Sun, and Yu Su. Mind2Web: Towards a Generalist Agent for the Web. *ArXiv*, abs/2306.06070, 2023.
- Charles Duhigg and A. Pole. How companies learn your secrets. 2012.
- Daniele Faraglia. Faker: A Python Package That Generates Fake Data, 2024. URL <https://github.com/joke2k/faker>.

- Arash Feizi, Shравan Nayak, Xiangru Jian, Kevin Qinghong Lin, Kaixin Li, Rabiul Awal, Xing Han Lù, Johan Obando-Ceron, Juan A. Rodriguez, Nicolas Chapados, David Vazquez, Adriana Romero-Soriano, Reihaneh Rabbany, Perouz Taslakian, Christopher Pal, Spandana Gella, and Sai Rajeswar. Grounding Computer Use Agents on Human Demonstrations, 2025. URL <https://arxiv.org/abs/2511.07332>.
- Boyu Gou, Ruohan Wang, Boyuan Zheng, Yanan Xie, Cheng Chang, Yiheng Shu, Huan Sun, and Yu Su. Navigating the Digital World as Humans Do: Universal Visual Grounding for GUI Agents. *ArXiv*, abs/2410.05243, 2024.
- Gretel AI. GLiNER Models for PII Detection through Fine-Tuning on Gretel-Generated Synthetic Documents, 10 2024.
- Ankush Gupta, A. Vedaldi, and Andrew Zisserman. Synthetic Data for Text Localisation in Natural Images. In *2016 IEEE Conference on Computer Vision and Pattern Recognition (CVPR)*, pp. 2315–2324, 2016.
- Behrooz Hashemian, Emanuele Massaro, I. Bojic, Juan Murillo Arias, Stanislav Sobolevsky, and C. Ratti. Socioeconomic characterization of regions through the lens of individual financial transactions. *PLoS ONE*, 12, 2017.
- Langdon Holmes, Scott Crossley, Harshvardhan Sikka, and Wesley Morris. PILO: An Open-Source System for Personally Identifiable Information Labeling and Obfuscation. *Information and Learning Sciences*, 124(9-10):266–284, 2023. doi: 10.1108/ILS-04-2023-0032.
- Yupan Huang, Tengchao Lv, Lei Cui, Yutong Lu, and Furu Wei. LayoutLMv3: Pre-training for Document AI with Unified Text and Image Masking. In *Proceedings of the 30th ACM International Conference on Multimedia*, 2022.
- JaiedAI. EasyOCR, 2024. URL <https://github.com/JaiedAI/EasyOCR>. Computer software.
- Orin S. Kerr. Buying data and the fourth amendment. Aegis Series Paper 2109, Hoover Institution, 2021. Available at SSRN: <https://ssrn.com/abstract=3880130>.
- Geewook Kim, Teakgyu Hong, Moonbin Yim, JeongYeon Nam, Jinyoung Park, Jinyeong Yim, Wonseok Hwang, Sangdoon Yun, Dongyoon Han, and Seunghyun Park. OCR-Free Document Understanding Transformer. In *European Conference on Computer Vision*, pp. 498–517, 2021.
- Michal Kosinski, D. Stillwell, and T. Graepel. Private traits and attributes are predictable from digital records of human behavior. *Proceedings of the National Academy of Sciences*, 110:5802 – 5805, 2013.
- Julien Lerouge, Guillaume Betmont, Thomas Bres, Evgeny Stepankevich, and Alexis Berges. DocXPand-25k: a large and diverse benchmark dataset for identity documents analysis. *ArXiv*, abs/2407.20662, 2024.
- Raymond Li, Loubna Ben Allal, Yangtian Zi, Niklas Muennighoff, Denis Kocetkov, Chenghao Mou, Marc Marone, Christopher Akiki, Jia Li, Jenny Chim, Qian Liu, Evgenii Zheltonozhskii, Terry Yue Zhuo, Thomas Wang, Olivier Dehaene, Mishig Davaadorj, J. Lamy-Poirier, João Monteiro, Oleh Shliazhko, Nicolas Gontier, Nicholas Meade, A. Zebaze, Ming-Ho Yee, Logesh Kumar Umapathi, Jian Zhu, Benjamin Lipkin, Muhtasham Oblokulov, Zhiruo Wang, Rudra Murthy, J. Stillerman, Siva Sankalp Patel, Dmitry Abulkhanov, Marco Zocca, Manan Dey, Zhihan Zhang, N. Fahmy, Urvashi Bhattacharyya, W. Yu, Swayam Singh, Sasha Luccioni, Paulo Villegas, M. Kunakov, Fedor Zhdanov, Manuel Romero, Tony Lee, Nadav Timor, Jennifer Ding, Claire Schlesinger, Hailey Schoelkopf, Jana Ebert, Tri Dao, Mayank Mishra, A. Gu, Jennifer Robinson, Carolyn Jane Anderson, Brendan Dolan-Gavitt, Danish Contractor, Siva Reddy, Daniel Fried, Dzmitry Bahdanau, Yacine Jernite, Carlos Muñoz Ferrandis, Sean M. Hughes, Thomas Wolf, Arjun Guha, L. V. Werra, and H. D. Vries. StarCoder: may the source be with you! *Trans. Mach. Learn. Res.*, 2023, 2023.
- Kevin Qinghong Lin, Linjie Li, Difei Gao, Zhengyuan Yang, Shiwei Wu, Zechen Bai, Weixian Lei, Lijuan Wang, and Mike Zheng Shou. ShowUI: One Vision-Language-Action Model for GUI Visual Agent, 2024.

- Yadong Lu, Jianwei Yang, Yelong Shen, and Ahmed Awadallah. OmniParser for Pure Vision Based GUI Agent. *ArXiv*, abs/2408.00203, 2024.
- Nils Lukas, Ahmed Salem, Robert Sim, Shruti Tople, Lukas Wutschitz, and Santiago Zanella-Béguelin. Analyzing Leakage of Personally Identifiable Information in Language Models. In *2023 IEEE Symposium on Security and Privacy (SP)*, pp. 346–363, 2023. doi: 10.1109/SP46215.2023.00038.
- Xing Han Lù, Zdeněk Kasner, and Siva Reddy. WebLINX: Real-World Website Navigation with Multi-Turn Dialogue. *ArXiv*, abs/2402.05930, 2024.
- Microsoft. Playwright, 2024a. URL <https://github.com/microsoft/playwright>.
- Microsoft. Presidio: Data Protection and De-identification SDK, 2024b. URL <https://github.com/microsoft/presidio>.
- Arvind Narayanan and Vitaly Shmatikov. Robust de-anonymization of large sparse datasets. *2008 IEEE Symposium on Security and Privacy (sp 2008)*, pp. 111–125, 2008.
- Milad Nasr, Nicholas Carlini, Jonathan Hayase, Matthew Jagielski, A. Feder Cooper, Daphne Ippolito, Christopher A. Choquette-Choo, Eric Wallace, Florian Tramèr, and Katherine Lee. Scalable Extraction of Training Data from (Production) Language Models. *ArXiv*, abs/2311.17035, 2023.
- OpenAI. GPT-4o mini: Advancing cost-efficient intelligence, July 2024. <https://openai.com/index/gpt-4o-mini-advancing-cost-efficient-intelligence/>.
- OpenAI. GPT-5 System Card Update: GPT-5.2. Technical report, OpenAI, December 2025. URL <https://openai.com/index/gpt-5-system-card-update-gpt-5-2/>.
- Vardaan Pahuja, Yadong Lu, Corby Rosset, Boyu Gou, Arindam Mitra, Spencer Whitehead, Yu Su, and Ahmed Awadallah. Explorer: Scaling Exploration-driven Web Trajectory Synthesis for Multimodal Web Agents. pp. 6300–6323, 2025.
- Naomi Sasaya, Shigefumi Kishida, Ryo Kikuchi, and Akira Tajima. Validating behavioral proxies for disease risk monitoring via large-scale e-commerce data. 2026.
- Sriram Selvam and Anneswa Ghosh. PANORAMA: A synthetic PII-laced dataset for studying sensitive data memorization in LLMs. *ArXiv*, abs/2505.12238, 2025.
- Ray Smith. An Overview of the Tesseract OCR Engine. In *Proceedings of the 9th International Conference on Document Analysis and Recognition (ICDAR 2007)*, volume 2, pp. 629–633. IEEE Computer Society, 2007. doi: 10.1109/ICDAR.2007.4376991.
- Aaron Sobel. End-running warrants: Purchasing data under the fourth amendment and the state action problem. *Yale Law & Policy Review*, 2023. Available at SSRN: <https://ssrn.com/abstract=4480782>.
- SST. OpenCode: The Open Source AI Coding Agent, 2025. URL <https://github.com/opencode-ai/opencode>.
- Amy Steier, Andre Manoel, Alexa Haushalter, and Maarten Van Segbroeck. Nemotron-PII: Synthesized Data for Privacy-Preserving AI, 2025. URL <https://huggingface.co/datasets/nvidia/Nemotron-PII>.
- Matthew J. Tokson. Government purchases of private data. *Wake Forest Law Review*, 59:269, 2024. University of Utah College of Law Research Paper No. 573.
- Andreas Veit, Tomas Matera, Lukás Neumann, Jiri Matas, and Serge J. Belongie. COCO-Text: Dataset and Benchmark for Text Detection and Recognition in Natural Images. *ArXiv*, abs/1601.07140, 2016.
- Haoming Wang, Haoyang Zou, Huatong Song, et al. UI-TARS-2 Technical Report: Advancing GUI Agent with Multi-Turn Reinforcement Learning, 2025a.

- Wenhao Wang, Zijie Yu, Rui Ye, Jianqing Zhang, Siheng Chen, and Yanfeng Wang. FedMABench: Benchmarking Mobile Agents on Decentralized Heterogeneous User Data. *ArXiv*, abs/2503.05143, 2025b.
- Wenhao Wang, Mengying Yuan, Zijie Yu, Guangyi Liu, Rui Ye, Tian Jin, Siheng Chen, and Yanfeng Wang. MobileA3gent: Training Mobile GUI Agents Using Decentralized Self-Sourced Data from Diverse Users. *Proceedings of the Fourth Workshop on Bridging Human-Computer Interaction and Natural Language Processing (HCI+NLP)*, 2025c.
- Xinyuan Wang, Bowen Wang, Dunjie Lu, Junlin Yang, Tianbao Xie, Junli Wang, Jiaqi Deng, Xiaole Guo, Yiheng Xu, Chen Henry Wu, Zhennan Shen, Zhuokai Li, Ryan Li, Xiaochuan Li, Junda Chen, Bo Zheng, Peihang Li, Fangyu Lei, Ruisheng Cao, Yeqiao Fu, Dongchan Shin, M. Shin, Jiarui Hu, Yuyan Wang, Jixuan Chen, Yuxiao Ye, Danyang Zhang, Dikang Du, Hao Hu, Hua Chen, Zaida Zhou, Haotian Yao, Ziwei Chen, Qizheng Gu, Yipu Wang, Heng Wang, Diyi Yang, Victor Zhong, Flood Sung, Y.Charles, Zhilin Yang, and Tao Yu. OpenCUA: Open Foundations for Computer-Use Agents. *ArXiv*, abs/2508.09123, 2025d.
- Zhaoyang Wang, Yiming Liang, Xuchao Zhang, Qianhui Wu, Siwei Han, Anson Bastos, Rujia Wang, Chetan Bansal, Baolin Peng, Jianfeng Gao, Saravan Rajmohan, and Huaxiu Yao. Adapting Web Agents with Synthetic Supervision. *ArXiv*, abs/2511.06101, 2025e.
- Tianbao Xie, Danyang Zhang, Jixuan Chen, Xiaochuan Li, Siheng Zhao, Ruisheng Cao, T. Hua, Zhoujun Cheng, Dongchan Shin, Fangyu Lei, Yitao Liu, Yiheng Xu, Shuyan Zhou, Silvio Savarese, Caiming Xiong, Victor Zhong, and Tao Yu. OSWorld: Benchmarking Multimodal Agents for Open-Ended Tasks in Real Computer Environments. *ArXiv*, abs/2404.07972, 2024.
- Jianwei Yang, Hao Zhang, Feng Li, Xueyan Zou, Chun yue Li, and Jianfeng Gao. Set-of-Mark Prompting Unleashes Extraordinary Visual Grounding in GPT-4V. 2023.
- Evan You. Vite, 2024. URL <https://github.com/vitejs/vite>.
- Shuyan Zhou, Frank F. Xu, Hao Zhu, Xuhui Zhou, Robert Lo, Abishek Sridhar, Xianyi Cheng, Yonatan Bisk, Daniel Fried, Uri Alon, and Graham Neubig. WebArena: A Realistic Web Environment for Building Autonomous Agents. *ArXiv*, abs/2307.13854, 2023.
- Zhi Zhou, Xu Chen, En Li, Liekang Zeng, Ke Luo, and Junshan Zhang. Edge Intelligence: Paving the Last Mile of Artificial Intelligence With Edge Computing. *Proceedings of the IEEE*, 107: 1738–1762, 2019.

Table 2: Comparison of PII detection benchmarks. WEBPII is the first to combine visual localization, semantic categories, web interface targeting, extended identifiers, and anticipatory form state support.

DATASET	DOMAIN	SIZE	VISUAL	SEMANTIC	WEB	EXT.	ANTIC.
AI4PRIVACY AI4PRIVACY (2023)	TEXT	300K	✗	✓	✗	✗	✗
PANORAMA SELVAM & GHOSH (2025)	TEXT	385K	✗	✓	✗	✗	✗
NEMOTRON-PII STEIER ET AL. (2025)	TEXT	100K	✗	✓	✗	✗	✗
GRETEL FINANCE GRETEL AI (2024)	TEXT	56K	✗	✓	✗	✗	✗
BIGCODE PII LI ET AL. (2023)	CODE	12K	✗	✓	✗	✗	✗
PIILO HOLMES ET AL. (2023)	ESSAYS	22K	✗	✓	✗	✗	✗
MIDV-2020 BULATOV ET AL. (2021)	ID DOCS	72K	✓	✓	✗	✗	✗
DOCXPAND-25K LEROUGE ET AL. (2024)	ID DOCS	25K	✓	✓	✗	✗	✗
COCO-TEXT VEIT ET AL. (2016)	SCENE	63K	✓	✗	✗	✗	✗
SYNTHTEXT GUPTA ET AL. (2016)	SCENE	800K	✓	✗	✗	✗	✗
WEBPII (OURS)	WEB UI	44K	✓	✓	✓	✓	✓

A DATASET STATISTICS

The dataset comprises 44,865 images spanning 10 e-commerce websites and 19 page types. Figure 4 visualizes form-fill variants, annotation density, category breakdown, and HTML element types. Figures 5–6 show company and page type distributions. Table 2 compares WEBPII against existing PII detection benchmarks.

The 52.4%/47.6% split between PII and non-PII annotations ensures models learn to distinguish sensitive user data from product and order metadata. Most annotations (78.1%) target rendered text rather than input fields (13.6%), reflecting that PII appears predominantly on confirmation and review pages where entered data is displayed, not just in the form fields where users type.

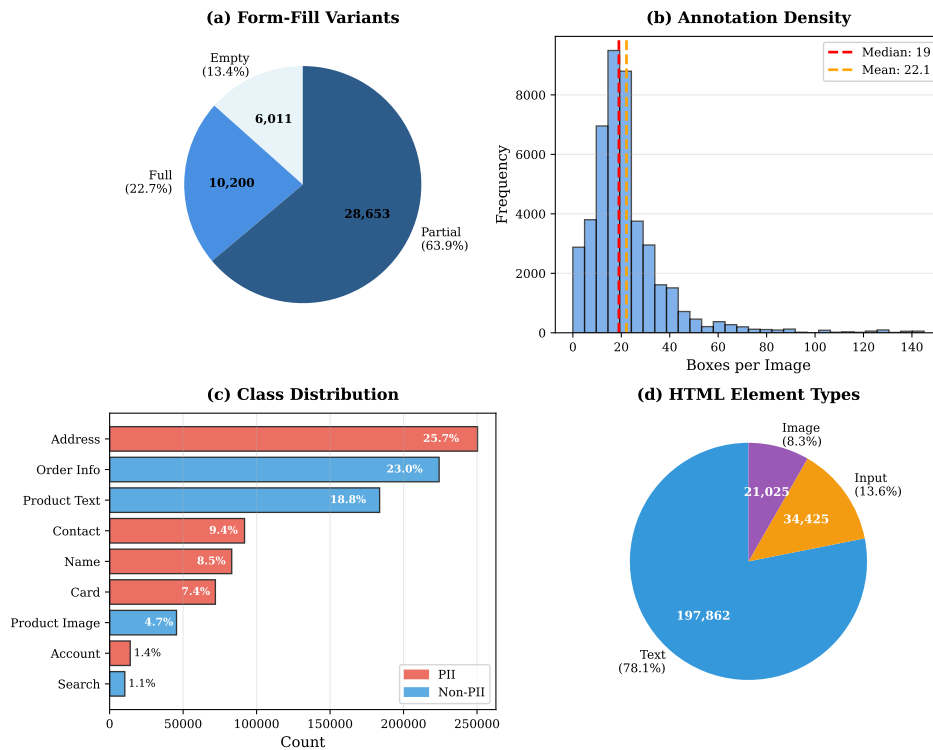


Figure 4: Dataset composition and statistics. (a) Distribution across form-fill variants—empty forms (13.4%), fully-filled forms (22.7%), and partial-fill states (63.9%)—enabling anticipatory detection training. (b) Annotation density distribution with median of 19 boxes per image (mean 22.1), ranging from 0 to 145 annotations per image. (c) Breakdown of all 9 annotation classes, with address (25.7%), order info (23.0%), and product text (18.8%) dominating. PII classes (red) comprise 52.4% of annotations, while non-PII classes (blue) comprise 47.6%. (d) HTML element type distribution, showing most annotations target rendered text (78.1%) versus input fields (13.6%) and images (8.3%).

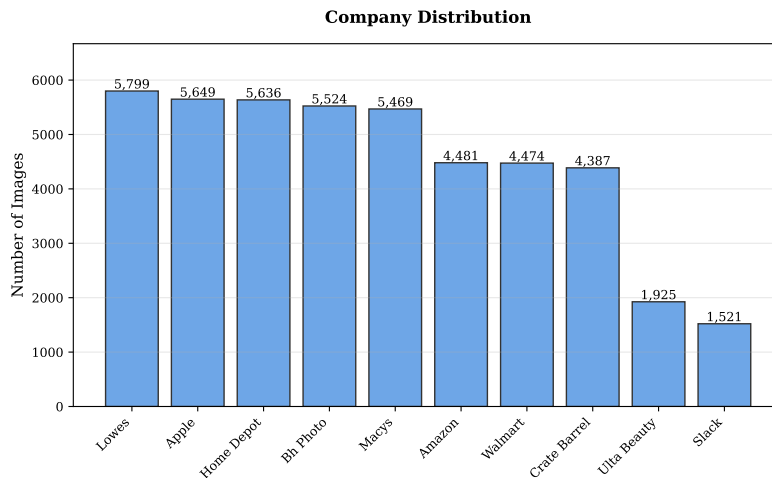


Figure 5: Distribution of base images across 10 e-commerce companies. Apple and Amazon have the most coverage (1,400 images each), while Slack and Ulta Beauty represent smaller verticals (300 images each). Total base images: 10,200 (multiplied across variants to produce 44,865 total dataset images).

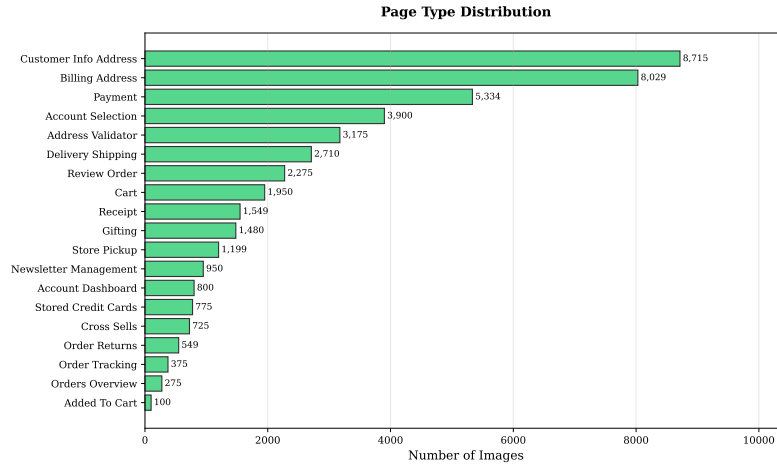


Figure 6: Distribution of base images across 19 page types spanning checkout flows, account management, and product pages. Account selection (900) and delivery/shipping (875) pages dominate, representing critical moments where PII exposure is highest.

B HUMAN QUALITY CONTROL PIPELINE

B.1 REVIEW INTERFACE AND WORKFLOW

Manually editing generated React code for hundreds of layouts would impose prohibitive overhead and require deep technical expertise. We instead developed a Flask-based web interface that accepts natural language correction instructions and delegates fixes to Claude. The interface operates on a queue system: layouts are displayed sequentially for review, with annotators able to examine the original screenshot, rendered reproduction, and all three annotated progressive fill states (empty, partial-fill, and fully-filled) to assess the full extent of data coverage. A code viewer provides access to the `App.jsx` source and `data.json` configuration for manual inspection when needed.

When an annotator identifies an issue, they submit a text instruction describing the required change. The system appends this instruction to a specialized fixing prompt that includes the current `App.jsx` source code, the original screenshot, and context from any previous fix iterations for that layout. Claude modifies the code and returns the corrected version. The interface then triggers re-rendering and re-annotation across all progressive fill states, allowing the annotator to verify the fix was applied correctly. Each layout underwent three review passes to ensure quality and provide redundancy in catching errors that might have been missed in earlier passes.

Refinement operates at the layout level rather than per-reproduction. Once a layout is corrected, the system re-screenshots across all three progressive fill states (empty, partial-fill, and fully-filled) to generate the final annotated dataset images, amortizing the cost of human review across multiple training samples.

We explicitly addressed the observed failure modes within the generation prompts themselves, providing specific instructions about viewport constraints, data attribute requirements, and form field initialization. However, rule-following remained imperfect for very nuanced cases—Claude would occasionally still produce viewport overflow or omit non-obvious data attributes despite explicit prompt guidance. Additionally, some errors were highly company-specific, and maintaining individually fine-tuned prompts per company would have undermined system scalability. We considered integrating more structured rubrics or checklists into the initial UI generation process to guide Claude through additional verification passes before human review. However, this would have introduced substantial costs through redundant forward passes that might not address the primary failure modes (viewport overflow detection, which requires human visual inspection, and context-dependent decisions about which non-obvious elements merit annotation). The conversational fixing interface proved more cost-effective by allowing targeted corrections only where needed rather than exhaustive verification on every layout.

B.2 REFINEMENT STATISTICS

The final dataset comprises 408 unique layouts. Of these, 160 (39.2%) required human-initiated refinements, totaling 312 individual correction iterations. Figure 7 shows the distribution of iterations required per layout. The majority (55.6%) needed only a single correction, while 21.9% required two iterations.

Total generation cost was \$649 using Claude Opus 4.5, comprising \$606 (93%) for initial reproduction and \$43 (7%) for refinements. This represents an average cost of \$1.50 per successfully generated layout including refinements, or \$1.41 per initial generation attempt. As expected, we observed notable variation according to page complexity.

Table 3 breaks down refinements by company and page type. Home Depot and Apple layouts required the most corrections (56 and 39 iterations respectively). Billing and payment pages accounted for 57 iterations across 29 layouts, the highest refinement density of any page type.

B.3 ERROR ANALYSIS AND FAILURE MODES

We manually categorized all 312 refinement iterations to understand failure modes (Figure 8). Four primary error categories emerged:

Table 3: Distribution of human-initiated refinements across companies and page types, ordered by total fixes.

CATEGORY	SAMPLES REFINED	TOTAL FIXES
<i>By Company</i>		
HOME DEPOT	22	56
LOWES	23	44
AMAZON	19	43
APPLE	25	39
MACY'S	13	39
BH PHOTO	21	33
WALMART	13	23
CRATE & BARREL	15	20
OTHERS	9	15
<i>By Page Type</i>		
BILLING/PAYMENT	29	57
CART	23	38
CUSTOMER INFO/ADDRESS	13	23
ADDRESS VALIDATOR	10	21
STORE PICKUP	8	20
ADDED TO CART	3	19
OTHERS	74	134
TOTAL	160	312

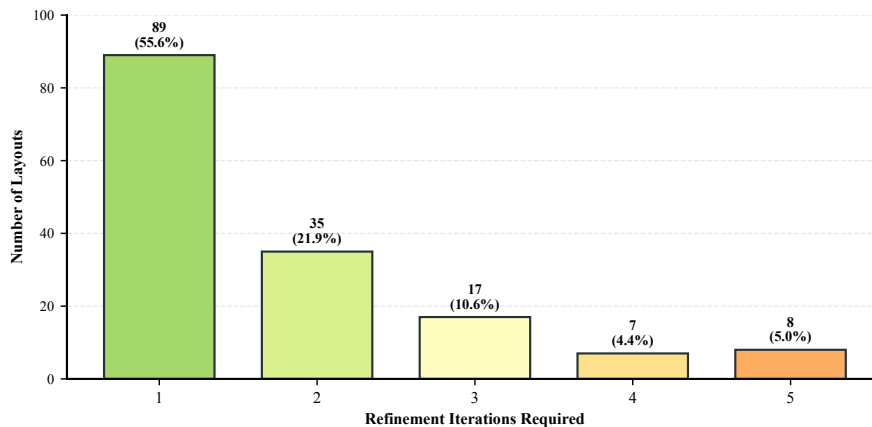


Figure 7: Distribution of refinement iterations required per layout across 160 layouts requiring refinement. Over half (55.6%) converged after a single correction iteration, while 21.9% required two iterations. Four layouts required more than 5 iterations.

Layout issues (53.8%). The dominant failure mode involved UI elements being pushed outside the viewport width due to incorrect responsive sizing or fixed-width constraints. Claude’s initial reproduction iterations included a visual refinement phase where a separate model invocation would compare rendered output to the original screenshot and suggest corrections. However, despite iterating over various prompts, Claude remained lacking robust spatial reasoning in images—when elements overflowed horizontally beyond the viewport boundary, the model could not detect the issue from the rendered screenshot alone. These errors required human annotators to identify clipped content (e.g., right-aligned cart summaries cut off at 1400px width, sidebar filters extending beyond viewport) and explicitly instruct Claude to adjust container widths or implement proper responsive constraints.

Missing or spurious data attributes (24.4%). These refinements predominantly involved product metadata fields like model numbers and item identifiers that were visually present but lacked proper `data-product` markup, likely do to the inapparent association with the general concept of PII. Apple interfaces exhibited a distinct failure mode: spurious `data-pii` or `data-product` attributes

added to decorative elements or redundant container divs that should not have been annotated. These false positive annotations required explicit removal instructions.

Incomplete fields (14.7%). Claude occasionally omitted input fields that did not match the common conceptual model of PII, requiring explicit addition instructions. A related issue involved selection dropdown defaults: Claude would sometimes hardcode dropdowns to specific values (e.g., “United States” for country selection) instead of initializing them to placeholder states (“Select a country”), which prevented proper partial-fill behavior where the dropdown should appear unselected. Note that certain fields were intentionally left unannotated—newsletter subscription email inputs, for example, were excluded from annotation as they represent marketing opt-ins rather than transaction-critical PII.

Hardcoded store locations (7.1%). Some layouts contained store-specific location references that were not necessarily the user’s personal location but could still be identifying or context-dependent—for example, “Presque Isle’s Lowes” in headers where the store location was not the key focus of the page. Claude initially rendered these as literal placeholder text rather than parametrizing them, requiring explicit correction.

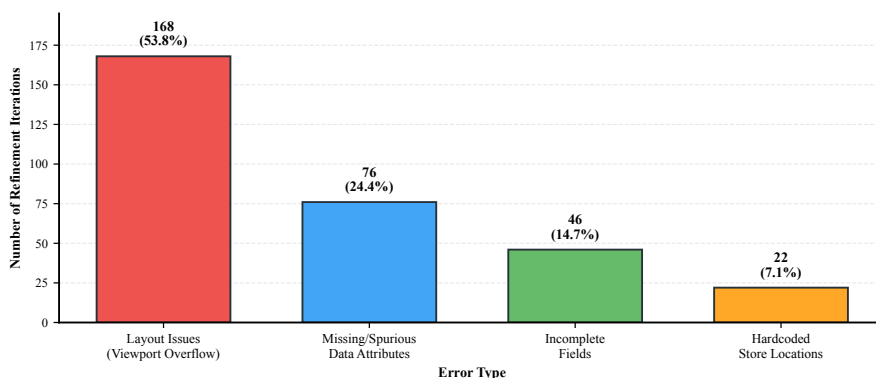


Figure 8: Breakdown of 312 refinement iterations by error type across 160 layouts. Layout issues (53.8%, primarily viewport overflow) dominated refinements. Data attribute errors (24.4%) involved spurious attributes on decorative components (particularly in Apple’s minimalist interfaces) and missing markup on product metadata fields. Incomplete fields (14.7%) included dropdown initialization issues. Hardcoded store locations (7.1%) required parametrization.

B.4 THROUGHPUT AND PIPELINE EFFICIENCY

The Claude-mediated generation and refinement pipeline achieved substantial throughput despite the human review requirement. A single annotator processed approximately 100 layouts per 2 hours during the review phase. This high throughput was enabled by several factors. First, Claude handled the majority of actual code modifications—the annotator’s role reduced to identifying errors and writing brief natural language correction instructions rather than performing manual code edits. Second, the interface provided immediate access to both the `App.jsx` source code and `data.json` configuration for manual inspection, allowing annotators to quickly diagnose issues by examining the underlying implementation. Third, the pipeline automated the full re-rendering and screenshot capture process—after submitting a fix, the system would rebuild the layout, capture screenshots across all three progressive fill states (empty, partial, full), run the annotation extraction, and present updated results within seconds. This fast iteration cycle eliminated manual overhead and enabled annotators to verify fixes immediately without context switching.

The primary bottleneck in dataset construction proved to be the collection of original e-commerce page screenshots rather than the generation or refinement process itself. Capturing diverse checkout flows, account dashboards, and payment pages across 10 major retailers required navigating authenticated sessions, filling realistic test data, and ensuring full-page screenshot capture across various UI states. Once source screenshots were collected, the automated pipeline consumed them rapidly. This architectural decision—delegating both generation and refinement to the model—proved essential for dataset feasibility, as manual HTML/CSS authoring or code-level debugging would have required orders of magnitude more human time.

C WEBREDACT-LARGE ABLATIONS

While WEBREDACT targets real-time inference at 30fps, WEBREDACT-LARGE prioritizes accuracy while maintaining near-real-time performance (~ 3 fps on CPU). This section provides complete analysis of WEBREDACT-LARGE trained at 1280×1280 resolution, including architectural comparisons, per-variant performance breakdowns, and inference latency measurements across hardware configurations.

C.1 ARCHITECTURE COMPARISON

Table 4 compares WEBREDACT and WEBREDACT-LARGE on $\text{Test}_{\text{Cross-Page}}$ with 10 text variants.

Table 4: Architecture comparison (2-class, cross-page, 10 text variants, trained on full+partial).

MODEL	RESOLUTION	MAP@50	PRECISION	RECALL
WEBREDACT	640×640	0.807	0.848	0.762
WEBREDACT-LARGE	1280×1280	0.909	0.868	0.834

WEBREDACT-LARGE achieves 0.909 mAP@50—a 12.6% relative improvement over WEBREDACT (0.807). Both precision and recall improve substantially (+2.0pp and +7.2pp respectively), indicating that higher resolution enables more accurate field boundary detection and reduces false positives.

C.2 PER-VARIANT PERFORMANCE

Table 5 shows per-variant performance breakdown for WEBREDACT-LARGE across test fill states.

Table 5: WEBREDACT-LARGE per-variant performance (2-class, cross-page, 10 text variants).

TEST VARIANT	MAP@50	PRECISION	RECALL
FULL	0.886	0.896	0.815
PARTIAL	0.943	0.897	0.878
EMPTY	0.898	0.809	0.809
AVERAGE	0.909	0.868	0.834

The model achieves particularly strong performance on partial-fill images (0.943 mAP@50), where the progressive fill training provides rich learning signal. Performance on fully-filled forms (0.886) is slightly lower, likely due to increased visual complexity when all fields contain text.

C.3 INFERENCE LATENCY

Table 6 compares inference latency between WEBREDACT and WEBREDACT-LARGE on both CPU and GPU hardware.

Table 6: Inference latency comparison (milliseconds per image).

MODEL	CPU (I5/RYZEN 5)	GPU (RTX 30XX)
WEBREDACT	~ 20 MS	< 5 MS
WEBREDACT-LARGE	~ 312 MS	~ 13 MS

WEBREDACT satisfies real-time constraints on CPU (< 33 ms per frame for 30fps), while WEBREDACT-LARGE requires 312ms (~ 3 fps)—nearly $16 \times$ slower but still suitable for near-real-time applications where higher accuracy justifies relaxed frame rate requirements. On GPU hardware, WEBREDACT-LARGE achieves 13ms latency, enabling real-time operation with GPU acceleration. For CPU-only deployment scenarios prioritizing maximum throughput, WEBREDACT remains the optimal choice.

D ADDITIONAL RESULTS

D.1 TEXT-BASED BASELINE DETAILS

D.1.1 DOCUMENT UNDERSTANDING MODELS VS. OCR PIPELINES

We compare three categories of text-based baselines on $\text{Test}_{\text{Cross-Company}}$ (Amazon, full-fill images): document understanding models (LayoutLMv3 Huang et al. (2022), Donut Kim et al. (2021)), OCR+LLM pipelines, and OCR+NER systems. Table 7 shows that document understanding models outperform simple OCR+LLM pipelines, with LayoutLMv3 achieving the highest $\text{mAP}@50$ (0.357) among all text-based approaches. To ensure fair comparison and bypass DocumentQA’s single-span extraction limitation, all document understanding pipelines use GPT-4o-mini for final classification after visual/layout encoding rather than extractive question answering.

Table 7: Document understanding models vs. OCR+LLM baselines on $\text{Test}_{\text{Cross-Company}}$ (Amazon, full-fill images). All methods use GPT-4o-mini for classification.

METHOD	MAP@50	PREC.	REC.	F1	LATENCY
LAYOUTLMV3 HUANG ET AL. (2022)	0.357	58.5%	45.1%	50.9%	2.9s
DONUT KIM ET AL. (2021)	0.350	55.8%	43.6%	48.9%	3.5s
TESSERACT SMITH (2007) + LLM	0.302	49.8%	49.6%	49.7%	2.8s

Document understanding models leverage visual layout information alongside text content, providing better localization on complex layouts like Amazon’s dense product grids and multi-column interfaces. However, this advantage remains modest (+18% $\text{mAP}@50$ over Tesseract Smith (2007)+LLM), and the architectural mismatch between word-level detections and field-level ground truth limits all text-based approaches.

D.1.2 OCR ENGINE ABLATION

Table 8 compares OCR engines with GPT-4o-mini classification. PaddleOCR Cui et al. (2025) achieves the highest precision (78.7%) but lowest recall (31.0%), while Tesseract Smith (2007) provides the best balance with competitive $\text{mAP}@50$ (0.302) at the fastest speed (2.8s). The narrow performance band (0.286–0.329 $\text{mAP}@50$) reveals that OCR quality is not the primary bottleneck—the architectural mismatch between word-level detections and field-level annotations limits all engines.

Table 8: OCR engine ablation with GPT-4o-mini classification.

OCR ENGINE	MAP@50	PREC.	REC.	F1	LATENCY
PADDEOCR CUI ET AL. (2025)	0.329	78.7%	31.0%	44.5%	6.6s
TESSERACT SMITH (2007)	0.302	49.8%	48.6%	49.2%	2.8s
EASYOCR JAIDEDAI (2024)	0.286	67.6%	30.7%	42.2%	3.8s

The classification latency (2.8–6.6s) is dominated by LLM inference rather than OCR extraction. Table 9 shows OCR-only latencies. Tesseract Smith (2007) completes in 453ms on CPU, while GPU-accelerated engines (EasyOCR JaiedAI (2024), PaddleOCR Cui et al. (2025)) are 1.6–4.7× slower despite hardware acceleration, indicating that OCR speed is not a primary bottleneck for text-based baselines, although still slower than our WEBREDACT and WEBREDACT-LARGE models.

Table 9: OCR engine latency (extraction only, no classification).

OCR ENGINE	LATENCY
TESSERACT SMITH (2007)	453MS
EASYOCR JAIDEDAI (2024)	715MS
PADDEOCR CUI ET AL. (2025)	2,143MS

D.1.3 OCR + PRESIDIO BASELINE

Table 10 shows OCR+Presidio performance across engines. Presidio’s rule-based NER achieves only 0.176–0.183 mAP@50, approximately 40% worse than LLM-based classification. Tesseract Smith (2007) provides the fastest configuration (1.3s), while PaddleOCR’s Cui et al. (2025) higher-quality extraction provides minimal benefit when the classifier lacks contextual understanding.

Table 10: OCR + Presidio NER (no LLM).

OCR ENGINE	MAP@50	PREC.	REC.	F1	LATENCY
TESSERACT SMITH (2007)	0.183	41.7%	26.3%	32.2%	1.3s
EASYOCR JAIDEDAI (2024)	0.178	42.1%	28.3%	33.9%	2.3s
PADLEOCR CUI ET AL. (2025)	0.176	44.5%	25.1%	32.1%	4.8s

D.1.4 DOCUMENT QUESTION ANSWERING

An alternative to LLM classification is Document Question Answering (DocQA), where models answer explicit questions like “What is the customer name?” to extract PII. We evaluate two pure DocQA approaches—Donut-DocVQA and LayoutLM with extractive QA heads—against the hybrid configurations (LayoutLMv3 + LLM, Donut + LLM) described above. Table 11 compares all approaches on Amazon test images.

Table 11: Document QA vs. LLM classification on Amazon test images.

METHOD	MAP@50	PREC.	REC.	F1	LATENCY
LAYOUTLMV3 HUANG ET AL. (2022) + LLM	0.357	58.5%	45.1%	50.9%	2.9s
DONUT KIM ET AL. (2021) + LLM	0.350	55.8%	43.6%	48.9%	3.5s
LAYOUTLM-QA	0.139	24.1%	47.8%	32.0%	1.5s
DONUT-DOCVQA	0.117	30.8%	37.7%	33.9%	11.5s

DocQA approaches fail for several reasons. First, DocVQA models are trained to extract single answer spans per question (e.g., “What is the date?” → “October 17”), not multiple items. This requires separate forward passes for each PII category (name, address, email, phone, card number, etc.), causing substantial latency: Donut’s OCR-free architecture processes the full image for each question at ~600ms per question (11.5s total), while LayoutLM’s extractive QA operates on pre-extracted OCR text more efficiently (1.5s total). Second, both models are pre-trained on structured documents and forms, where PII appears in predictable locations with clear visual cues (labeled fields, tables). E-commerce screenshots present different visual hierarchies—gift recipient versus billing names, optional fields, promotional overlays—that deviate from the models’ training distribution. Third, rigid question templates often mismatch actual page content, requiring flexible contextual understanding that the single-span extraction paradigm cannot provide. Fourth, LayoutLM-QA uses a randomly initialized QA head (not fine-tuned), further degrading span extraction quality.

LLM classification (sending all extracted text to GPT-4o-mini for contextual classification) achieves 2.6× higher mAP@50 (0.357 vs 0.139) than the best DocQA method while maintaining comparable or faster speed. The flexible classification paradigm handles diverse layouts without rigid question templates.

D.1.5 FAILURE MODES

The two-stage architecture creates cascading errors where OCR misdetections propagate to classification. On sparse pages with few ground truth elements, OCR misreads generic footer text or company names, causing the LLM to aggressively flag these undetected strings as sensitive and producing false positives. Conversely, dense pages with complex product listings cause context rot in chunked LLM calls, where the model loses track of relevant fields as listings overwhelm the limited context window. Product names containing person names (e.g., “Kelsey Villages” as a street name versus “Kelsey” as a brand) are frequently misclassified, and gift messages containing potentially private data are sometimes missed.

D.1.6 CLASSIFICATION PROMPT

The OCR + LLM baselines use GPT-4o-mini to classify extracted text spans. The classification prompt is:

```
You identify data values in e-commerce screenshot text.
Flag ANY text that is actual data (not a UI label):
Names, addresses, cities, states, zip codes
Emails, phone numbers, dates
Card numbers, CVV, expiry dates
Product names, brands, prices, quantities, ratings
Order totals, shipping costs, tracking numbers
Search queries, gift messages
Only skip pure UI labels like "Price:", "Quantity:", "Add to
cart".
When in doubt, include it.
Return JSON: {"pii.items": [{"text": "exact text"}]}
```

D.2 PER-CLASS PERFORMANCE BREAKDOWN

Table 12 shows per-class AP@50 on fully-filled test images across split strategies for 2-class detection.

Table 12: Per-class AP@50 on fully-filled test images (test_full variant).

SPLIT	TEXT	IMAGE
CROSS-PAGE	0.623	0.870
CROSS-COMPANY	0.471	0.855
CROSS-TYPE	0.552	0.875

Product images achieve robust detection across all splits (0.855–0.875 AP@50), confirming that visual elements have distinctive signatures that generalize well regardless of company branding or page type. Text detection shows more variation: cross-page performance reaches 0.623 AP@50, while cross-company and cross-type splits achieve 0.471 and 0.552 AP@50 respectively. This degradation reflects the challenge of generalizing text field detection when visual styling (borders, fonts, spacing) varies across unseen companies or form types.

D.3 SPLIT STRATEGY ABLATION

Table 13 compares three split strategies that evaluate generalization at different levels. $\text{Test}_{\text{Cross-Page}}$ achieves the strongest average performance (0.797 mAP@50), with particularly high partial-fill detection (0.842), indicating that models learn layout-invariant features within a company’s design system. $\text{Test}_{\text{Cross-Company}}$ degrades to 0.753 when generalizing to Amazon’s distinct visual style, with the largest drop on full-fill images (0.663) where dense product layouts and unique styling present the greatest challenge. $\text{Test}_{\text{Cross-Type}}$ shows the most uniform degradation across fill states (0.713–0.744), revealing that page-type-specific patterns—such as dense tabular receipts versus interactive checkout forms—transfer less effectively than company-specific design conventions.

Table 13: Split strategy comparison (WEBREDACT, 2-class, trained on full+partial). $\text{Test}_{\text{Cross-Page}}$ performs best, while $\text{Test}_{\text{Cross-Type}}$ presents the strongest generalization challenge.

SPLIT STRATEGY	FULL	PARTIAL	EMPTY	AVG
$\text{TEST}_{\text{CROSS-PAGE}}$	0.747	0.842	0.803	0.797
$\text{TEST}_{\text{CROSS-COMPANY}}$	0.663	0.839	0.756	0.753
$\text{TEST}_{\text{CROSS-TYPE}}$	0.713	0.727	0.744	0.728

D.4 FILL STATE ABLATION

Table 14 ablates training data composition to isolate the contribution of each fill state. Training on full screenshots alone achieves 0.771 mAP@50. Counterintuitively, adding empty screenshots *without* partials degrades performance to 0.758, likely because the visual gap between empty forms (placeholder text, unfilled fields) and fully-filled forms is too large for the model to bridge without intermediate examples. Adding partial-fill data resolves this: full+partial achieves 0.797 (+0.026 over full-only), with the strongest gains on partial test images (0.842 versus 0.810), confirming that mid-entry states provide essential visual grounding. Combining all three states achieves the best overall performance (0.825 mAP@50), demonstrating that empty forms become useful once partial fills provide the intermediate signal that bridges the visual gap.

Table 14: Fill state ablation on Test_{Cross-Page} (WEBREDACT, 2-class). Partial-fill data is essential; empty screenshots help only when combined with partials.

TRAIN	FULL	PART.	EMPTY	AVG
EMPTY	0.672	0.818	0.777	0.756
FULL	0.736	0.810	0.767	0.771
FULL+EMPTY	0.734	0.774	0.768	0.758
FULL+PART.	0.747	0.842	0.803	0.797
FULL+PART.+EMPTY	0.762	0.881	0.831	0.825

D.5 PROGRESSIVE FILL DENSITY ABLATION

We ablate the number of partial-fill screenshots per layout to measure how progressive completion stages affect model performance. Each layout generates multiple partial-fill variants representing different stages of form completion. We evaluate 1, 3, and 5 partial stages; higher sampling counts would effectively approximate capturing all possible intermediate states (e.g., sampling 7 partials from a 7-field form would capture every field-by-field completion step).

Table 15: Progressive fill density ablation (WEBREDACT, 2-class, cross-page, trained on full+partial). Shows per-variant breakdown and overall metrics.

PARTIALS	TRAIN	TEST_FULL	TEST_PARTIAL	TEST_EMPTY	AVG MAP	PREC.	REC.
1	521	0.727	0.774	0.774	0.758	0.793	0.688
3	763	0.738	0.794	0.779	0.770	0.811	0.709
5	938	0.762	0.835	0.810	0.802	0.822	0.727

Performance improves consistently with more partial stages, increasing from 0.758 mAP@50 (1 partial) to 0.802 (5 partials), with gains across all test variants. Both precision and recall improve (0.793 to 0.822 and 0.688 to 0.727 respectively), demonstrating that each progressive completion stage provides non-redundant learning signal. The model shows particularly strong gains on test_{partial} images (0.774 to 0.835), confirming that training on multiple intermediate form-filling states enables more robust field detection patterns.

D.6 DATA VARIANT ABLATION DETAILS

We ablate the number of text variants per layout to measure how data diversity affects generalization. Each unique layout is rendered with 1, 10, or 25 distinct PII data injections (varying names, addresses, products, etc.).

Performance improves consistently with more text variants, rising through 0.795, 0.811, and 0.820, demonstrating that the injectable data system successfully provides training diversity beyond layout diversity alone. Both precision and recall increase with more variants (0.805 to 0.842 and 0.713 to 0.731 respectively). The model shows particularly strong gains on test_{partial} images (0.831 to 0.866), confirming that diverse PII data injections (varying names, addresses, products) enable the model to learn more robust patterns that generalize across different data instances.

Table 16: Text variant ablation on Test_{Cross-Page} (WEBREDACT, 2-class, trained on full+partial). Shows per-variant breakdown and overall metrics.

VARIANTS	TEST_FULL	TEST_PARTIAL	TEST_EMPTY	AVG MAP	PREC.	REC.
1	0.762	0.831	0.791	0.795	0.805	0.713
10	0.774	0.856	0.804	0.811	0.829	0.722
25	0.783	0.866	0.812	0.820	0.842	0.731

D.7 QUALITATIVE PREDICTION ANALYSIS

Figure 9 shows prediction patterns for WEBREDACT and WEBREDACT-LARGE on cross-page test images. Both models demonstrate strong performance on core detection targets: all input fields, product images, and prices achieve near-perfect detection. These well-represented patterns in the training data are reliably captured.

Failures predominantly occur on underrepresented edge cases. The top image exhibits numerous false positives (red boxes), where the model over-detects elements that the ground truth does not annotate. WEBREDACT also annotates promotional text like “Save up to 15% on future auto deliveries”, which represents marketing content rather than user-specific information. These false positives indicate the model responds to certain visual contexts (callouts, banners, emphasized text) where distinguishing promotional content from actual data fields remains challenging. Missed detections (blue boxes) occur when PII appears in atypical visual presentations: the recipient name “Gregory” rendered as a large bold callout at the top of the page rather than within a standard form field, and delivery dates like “Tuesday, May 18” styled in green text rather than conventional black typography. The bottom image shows detection patterns on a payment page, where both models successfully capture most standard form fields but exhibit characteristic failures. WEBREDACT misses hard-to-notice form fields without observable borders when empty, and both models struggle with small numbers in densely packed locations like “2 item” quantity indicators. Both models also produce false positives on an unlabeled dropdown menu—though this reflects legitimate annotation ambiguity, as the same dropdown could reasonably be tagged if rendered with a visible selected value. Despite these edge case failures, form field detection remains robust overall. These failures reflect the dataset’s composition: while training data spans diverse e-commerce contexts, forms and cart pages dominate and establish the primary visual patterns for input fields, product images, and prices. The model learns these dominant patterns robustly but struggles when sensitive information appears in more information-dense or ambiguous contexts.

To assess generalization to non-synthetic data, we qualitatively evaluated the model on the original e-commerce screenshots used as generation targets, as well as 50 additional real e-commerce screenshots that were never synthetically reproduced from the same brands. We do not release these images due to their sensitive content. Upon observing the annotations, we recognize that input fields, prices, and product details demonstrate robust detection across varied contexts, confirming that patterns learned from synthetic reproductions transfer to authentic interfaces. However, shipping dates, cardholder names rendered on card images, and basket quantities exhibit inconsistent detection, consistent with the underrepresentation patterns observed on synthetic test data demonstrated in Figure 9.

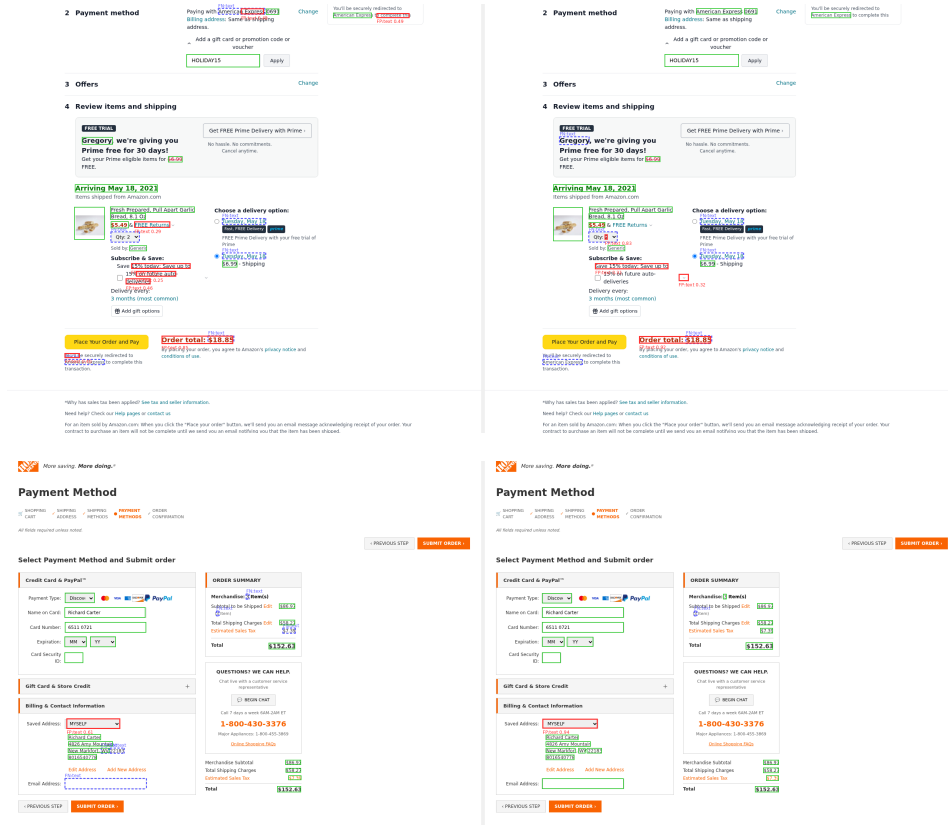


Figure 9: Qualitative comparison of WEBREDACT (left) and WEBREDACT-LARGE (right) predictions on cross-page test images. Green boxes indicate correct alignment with ground truth, red boxes indicate false positives, and blue boxes indicate false negatives.